Metal layer Bragg–Fresnel lenses for diffraction focusing of hard x-rays

Youli Li,[a] Mario Yasa, Olivier Pelletier, and Cyrus R. Safinya
Materials Research Laboratory, Materials and Physics Departments, University of California, Santa Barbara, California 93106

Ernie Caine and Evelyn E. Hu
Electrical and Computer Engineering Department, National Nanofabrication Users Network (NNUN) and California NanoSystems Institute (CNSI), University of California, Santa Barbara, California 93106

Patricia Fernandez
The Advanced Photon Source, Argonne National Laboratory, Argonne, Illinois 60439

(Received 7 November 2002; accepted 18 February 2003)

A thin-film Bragg–Fresnel lens (BFL) was developed for diffractive focusing of hard x-rays into submicron to nanometer spots for scanning x-ray spectromicroscopy. The lens is made of metal-layer Fresnel zones deposited on an x-ray reflective substrate. The use of a high-density lens structure reduces the thickness of the lens and simplifies the fabrication process. Linear and elliptical lenses made of a 200-nm-thick Au film were fabricated using e-beam lithography and a metal deposition process. The focusing capabilities of the Au layer BFLs were demonstrated at the Advanced Photon Source. © *2003 American Institute of Physics*. [DOI: 10.1063/1.1567456]

Diffractive x-ray micro-optics based on Fresnel zone-plate (ZP) structures have been widely used to generate submicron, hard x-ray (wavelength 0.1 Å–10 Å) microprobes for x-ray spectromicroscopy and microdiffraction applications.[1–5] Two types of Fresnel ZPs are commonly used in the hard x-ray regime: the transmission ZP and the Bragg–Fresnel lens (BFL).[5,6] The transmission ZPs are effective and relatively easy to use, but are difficult to fabricate due to the high feature aspect ratio of the lens structure.[5,7] The reflection BFL requires only a fraction of the zone thickness of a transmission ZP because the oblique-incidence reflection geometry effectively amplifies the x-ray path length.[6,8] Here, we report a heterostructure BFL made of metallic thin-film Fresnel zones deposited on a silicon substrate. Unlike single crystal BFLs, which are made by a subtractive etching process, the metal-layer BFLs (ML-BFLs) are fabricated by using a simpler, additive metal deposition process. The lens structure in principle can be made on any x-ray reflective substrate (e.g., single crystals, mirrors, and multilayers), therefore making possible x-ray focusing elements combining geometric and diffractive focusing mechanisms.

The structure of a ML-BFL is shown in Fig. 1(a). The phase retardation caused by the metalized Fresnel zones is dependent on the path length of the x rays in the layer as well as the index of refraction of the layer material:

$$\Delta\phi = \frac{4\pi h\delta}{\lambda \sin\theta} = \frac{8\pi h\delta d_{hkl}}{\lambda^2}, \tag{1}$$

where λ is the wavelength of the radiation, $n = 1-\delta+i\beta$ the index of refraction of the layer material, and d_{hkl} the Bragg plane spacing of the substrate. The lens layer thickness is determined by setting $\Delta\phi = \pi$ in Eq. (1):

$$h = \frac{\lambda^2}{8 d_{hkl}\delta}. \tag{2}$$

Away from resonant absorption edges, $\delta \propto \rho\lambda^2$, where ρ is the density of the material. Equation (2) shows that the layer thickness is inversely proportional to the density and is approximately independent of the wavelength except in the vicinity of an absorption edge. This latter property enables BFLs to be used to focus x rays in a broad energy range without significant loss in efficiency.

In order to reduce the thickness of the lens, it is necessary to use high-density materials. In a traditional BFL, in which the lens layer is made of the same material as the substrate, the use of higher density substrates, such as GaAs and Ge, has been exploited to reduce the zone thickness.[8,9] In the heterostructured ML-BFL, however, the high-density lens-layer material can be chosen independent of the substrate, which can yield a significant reduction in the lens thickness. For example, at 8 keV the zone thicknesses of Au, W, and P_t ML-BFLs on Si (111) substrates are 201, 204, and 182 nm, respectively. In contrast, a single-crystal Si (111) BFL has a zone thickness of $\sim$1280 nm.

It is necessary to consider the performance of ML-BFLs near absorption edges as the heavy metals used for the lens layer typically have L edges in the energy range (10–18 keV) that the BFLs are commonly used in. The abrupt change in the complex index of refraction at or near the absorption edge will have two effects: the change in δ will result in a deviation from the desired phase shift π and the variation in β will result in a different absorption loss in the lens layer. In Fig. 1(b), we show as a function of photon energy the calculated phase shift and transmission in a 200-nm-thick Au layer BFL on a Si (111) substrate. The calculation was done based on tabulated values of δ and β, both of which change dramatically at the L_I–L_{III} absorption edges. The peak deviation from optimal phase shift is 18% ($\Delta\phi = 0.82\pi$) at the Au L_{III} edge. We note that, although this

[a]Author to whom correspondence should be addressed; electronic mail: youli@mrl.ucsb.edu

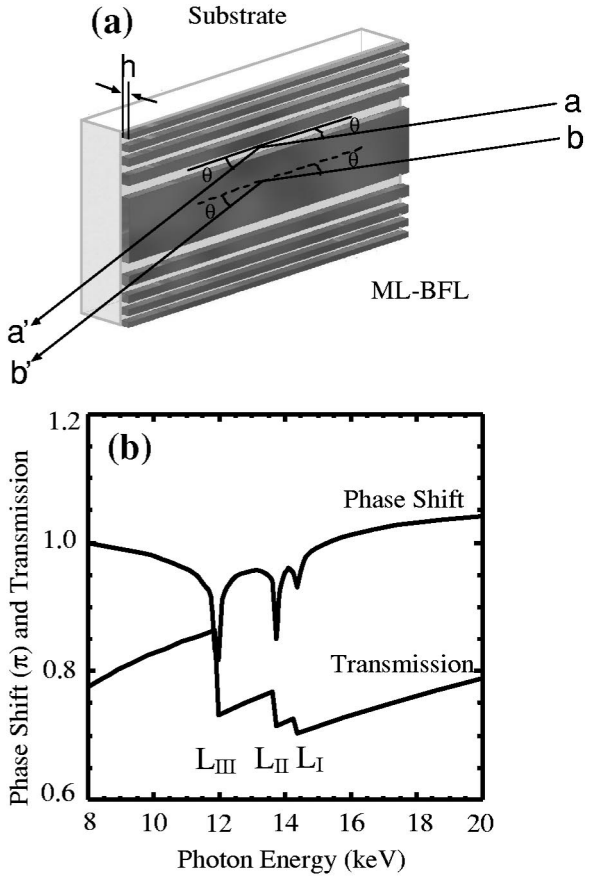

FIG. 1. (a) The structure of a linear ML-BFL. X rays reflected by the single-crystal substrate through the metalized Fresnel zones are phase shifted due to the density difference between the metal layer and air. (b) Phase shift in the metal layer and overall transmission of an Au layer ML-BFL as a function of photon energy. Dramatic changes occur at the three L edges of Au.

deviation will result in a reduction in lens efficiency, the drop will be at most smaller than 9%, simply due to the fact that only half the zones are metallized. The transmission of the lens layer is defined as $(1-A_m\alpha/A)$, where A_m, α, and A are the total area of the metallized zones, the absorption coefficient of the metal layer, and the total area of the lens, respectively. The maximum and minimum transmissions are 86% and 70%, respectively, which occur at just below and above the Au L_{III} edge. To minimize changes in lens efficiency, one could choose an operating energy away from the absorption edges.

The fabrication process of the ML-BFLs consists of two main steps: pattern (zone) definition by electron-beam lithography and pattern formation by e-beam evaporation. Fresnel patterns were written with a JEOL JBX-5DII e-beam writer on Si (111) substrates coated with a standard poly (methylmethacrylate) resist layer. After pattern development, the sample was placed in an e-beam evaporator and coated with 200 nm of Au on top of a 10-nm Ti buffer layer. Compared to the fabrication of single crystal BFLs,[8] this process is less complicated due to the elimination of the etching step. The Ti buffer layer was used to enhance adhesion of the device layer and has a negligible effect on lens properties because of its low density. We show in Fig. 2 two scanning electron microscope (SEM) images of the Au linear and elliptical ML-BFLs fabricated on Si (111) substrates. The lenses have

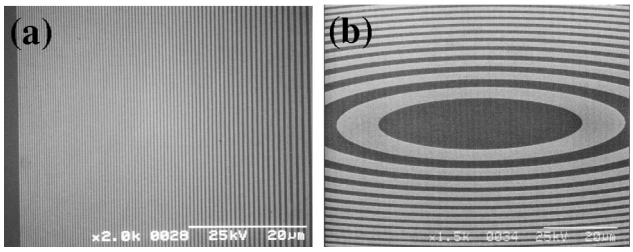

FIG. 2. SEM images of linear (a) and elliptical (b) Au ML-BFLs. The zone width at the edge of the device and the lens layer thickness are both 200 nm.

outermost zone widths of 200 nm, and several lenses with focal lengths between 25 and 75 CM for 12-keV x rays were produced on one substrate. The linear lenses have a 20-mm zone length. The elliptical lenses have a long/short axis ratio that is dependent on the Bragg angle: $b/a=1/\sin\theta$. For Si (111) lenses at 12 keV, this ''stretching factor'' is about 6.

X-ray characterization of the ML-BFLs was conducted at beamline 1-ID at the Advanced Photon Source (APS) at Argonne National Laboratory. The experiments were conducted at 12 keV, which is just above the Au L_{III} edge. At this energy, the 200-nm Au layer produces about 0.82π of phase shift and the lens has an overall transmission of 73%. To directly observe the beam, we used an x-ray video microscope consisting of a 100-μm-thick $CdWO_4$ scintillation screen, a 10× microscope objective, and a CCD video camera. As the BFL was moved into the incident beam, a sharp, intense focal spot could be seen on the video screen. In Figs. 3(a) and 3(b), we show captured video images of the beam as the linear and elliptical BFLs were moved into the beam. From left to right, the images show, sequentially, the beam profiles when the BFLs were outside of the beam, partially in the beam, and centered in the beam.

To measure the beam profile precisely we used the x-ray fluorescence emission from well-defined microstructures as they were being scanned through the focused x-ray beam.[10] A 5-μm-wide Ni strip (length=5 mm) supported by a Si wafer was used to sample the line focused beam produced by the linear BFL. An energy dispersive Si PIN diode detector (Amptek XR-100CR) with a multichannel analyzer was used to measure the K-shell fluorescence from the Ni strip. The intensity profile of the line-focused beam is shown in Fig. 3(b). The full-width at half-maximum (FWHM) of the central peak is 5.68 μm, which is mostly due to the 5-μm aperture function. Because the edge of the photolithography-defined Ni strip is sharp (roughness <10 nm), we could treat the rising and falling edges of the peak as knife-edge scans, for which the FWHM of the peak can be taken as the width between 25% and 75% intensity levels. The focus size derived using this method is 1.4 μm, which is approximately 2× the expected focus size of 0.75 μm determined by source demagnification (the undulator source size is 150 μm at 60 m upstream from the BFL, which has a focal length of 30 cm). This focus broadening most likely resulted from the misalignment of the Fresnel zones with respect to the incident beam.

For elliptical BFLs, we used a 5-μm×5-μm Ni film on a Si wafer to measure the two-dimensional beam profile, which is shown in Fig. 3(d). We estimated the true focus size by taking vertical and horizontal traces across the beam cen-

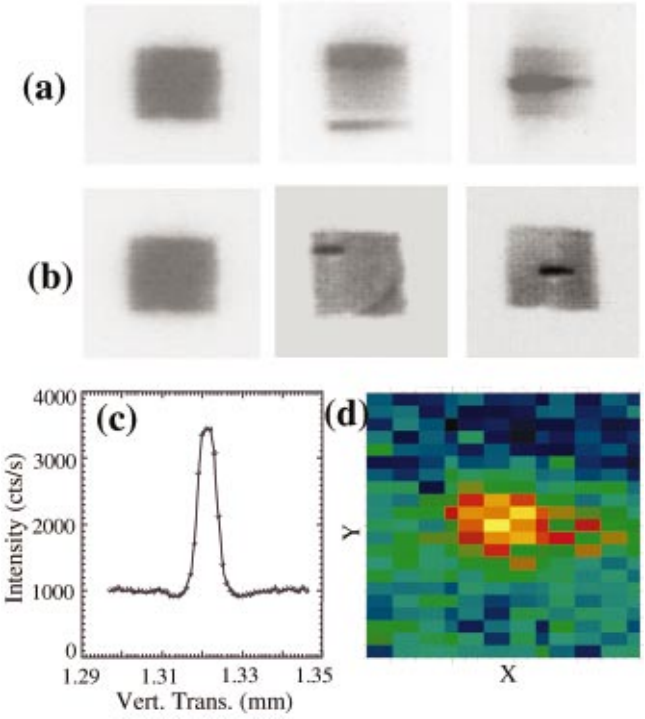

FIG. 3. (Color) X-ray focusing data collected at beamline 1-ID at APS from linear and elliptical ML-BFLs. (a), (b) X-ray video microscope images of the x-ray beam at the focal plane of a linear (a) and an elliptical (b) ML-BFL, respectively, showing (from left to right): the unfocused beam, the partially focused beam, and the focused beam. The shadows of the lenses are visible in the middle images when the BFLs are partially in the beam. (c) The vertical intensity profile at the focus of a linear ML-BFL mapped using the x-ray fluorescence from a 5-μm Ni strip. (d) Two-dimensional intensity map of the focused beam generated by the elliptical ML-BFL. The data were collected using x-ray fluorescence from a 5-μm$\times$5-μm Ni square raster scanned through the beam. Pixel size is 2 μm (horizontal) $\times$1 μm (vertical).

ter. Assuming the observed focus as the result of a convolution of two Gaussian profiles (focused beam and the sampling aperture), the focus size was then estimated using the formula $w_f^2 = w_p^2 - w_a^2$, where w_a is the width of the aperture (5 μm), w_p the width of the observed peak, and w_f the focus size. We arrived at a focus size of 1.8 μm (vertical) $\times$7.5 μm (horizontal), which is again within a factor of 2 of the demagnified source (horizontal source size is $\sim 5\times$ larger than vertical).

We are currently developing two methods to study structures of complex fluids and biological macromolecules in confined geometries using the ML-BFL-generated x-ray microprobe. One method involves the use of microchannels that can induce alignment of filamentous proteins on a microarray substrate.[11] Another method utilizes the x-ray surface forces apparatus, which allow *in-situ* x-ray diffraction studies of fluid samples under confinement and shear.[12] The line-focused beam produced by using a linear ML-BFL was used in a microbeam small-angle diffraction setup to probe the structure of fluid membranes under surface confinement in a 100-μm rectangular capillary. The use of the microprobe of order 1 μm allowed us to map the orientation of the membranes as a function of the separation between the membrane domain and the confining surface.[13]

We gratefully acknowledge support by National Science Foundation grant DMR-0076357, Office of Naval Research Grant N00014-00-1-0214, and UC-Los Alamos National Laboratory Grant No. 45909-0012-2P. This work was partially supported by the MRSEC program of the National Science Foundation under Award No. DMR00-80034. Use of the APS was supported by U.S. Department of Energy, Basic Energy Sciences, Office of Energy Research, under Contract No. W-31-109-Eng-38.

[1] A. Firsov, A. Svintsov, A. Erko, W. Gudat, A. Asryan, M. Ferstl, S. Shapoval, and V. Aristov, Nucl. Instrum. Methods Phys. Res. A **467**, 366 (2001).
[2] C. David and A. Souvorov, Rev. Sci. Instrum. **70**, 4168 (1999).
[3] E. Di Fabrizio, F. Romanato, M. Gentili, S. Cabrini, B. Kaulich, J. Susini, and R. Barrett, Nature (London) **401**, 895 (1999).
[4] W. Leitenberger, T. Weitkamp, M. Drakopoulos, I. Snigireva, and A. Snigirev, Opt. Commun. **180**, 233 (2000).
[5] W. Yun, B. Lai, Z. Cai, J. Maser, D. Legnini, E. Gluskin, Z. Chen, A. A. Krasnoperova, Y. Vladimirsky, F. Cerrina, E. Di Fabrizio, and M. Gentili, Rev. Sci. Instrum. **70**, 2238 (1999).
[6] A. Snigirev, Rev. Sci. Instrum. **66**, 2053 (1995).
[7] A. A. Krasnoperova, J. Xiao, F. Cerrina, E. Difabrizio, L. Luciani, M. Figliomeni, and M. Gentili, J. Vac. Sci. Technol. B **11**, 2588 (1993).
[8] Y. Li, G. C. L. Wong, C. R. Safinya, E. Caine, E. L. Hu, D. Haeffner, P. Fernandez, and W. Yun, Rev. Sci. Instrum. **69**, 2844 (1998).
[9] A Souvorov, A. Snigirev, I. Snigireva, and E. Aristova, Rev. Sci. Instrum. **67**, 1733 (1996).
[10] Y. Li, G. C. L. Wong, R. Case, C. R. Safinya, E. Caine, E. Hu, and P. Hernandez, Appl. Phys. Lett. **77**, 313 (2001).
[11] T. Pfohl, J. H. Kim, M. Yasa, H. P. Miller, G. C. L. Wong, F. Bringezu, Z. Wen, L. Wilson, M. W. Kim, Y. Li, and C. R. Safinya, Langmuir **17**, 5343 (2001).
[12] Y. Golan, M. Seitz, C. Luo, A. Martin-Herranz, M. Yasa, Y. Li, C. R. Safinya, and J. Israelachvili, Rev. Sci. Instrum. **73**, 2486 (2002).
[13] Y. Li, Y. Golan, A. Martin-Herranz, O. Pelletier, M. Yasa, J. N. Israelachivili, and C. R. Safinya, Int. J. Thermophys. **22**, 1175 (2001).